NANO LETTERS

LETTER

pubs.acs.org/NanoLett

Locally Oxidized Silicon Surface-Plasmon Schottky Detector for Telecom Regime

Ilya Goykhman,[†,§] Boris Desiatov,[†,§] Jacob Khurgin,[‡] Joseph Shappir,[†] and Uriel Levy*[,†]

[†]Department of Applied Physics, The Benin School of Engineering and Computer Science, The Center for Nanoscience and Nanotechnology, The Hebrew University of Jerusalem, Jerusalem, 91904, Israel

[‡]Department of Electrical and Computer Engineering, Johns Hopkins University, Baltimore Maryland 21218, United States

ABSTRACT: We experimentally demonstrate an on-chip nanoscale silicon surface-plasmon Schottky photodetector based on internal photoemission process and operating at telecom wavelengths. The device is fabricated using a self-aligned approach of local-oxidation of silicon (LOCOS) on silicon on insulator substrate, which provides compatibility with standard complementary metal-oxide semiconductor technology and enables the realization of the photodetector and low-loss bus photonic waveguide at the same fabrication step. Additionally, LOCOS technique allows avoiding lateral misalignment between the silicon surface and the metal layer to form a nanoscale Schottky contact. The fabricated devices showed enhanced detection capability for shorter wavelengths that is attributed to increased probability of the internal photoemission process. We found the responsivity of the nanodetector to be 0.25 and 13.3 mA/W for incident optical wavelengths of 1.55 and 1.31 μm, respectively. The presented device can be integrated with other nanophotonic and nanoplasmonic structures for the realization of monolithic opto-electronic circuitry on-chip.

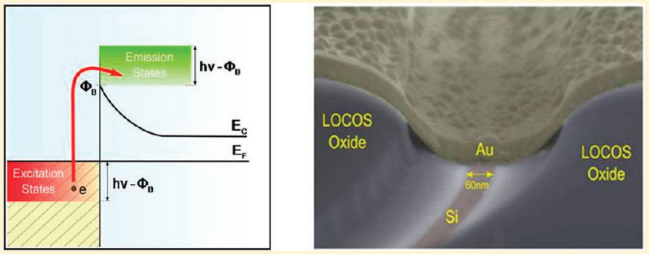

KEYWORDS: Local-oxidation, Schottky-detector, silicon-photonics, surface-plasmons, internal photoemission

In the past two decades, we have been witnessing a rapid progress in toward the realization of complementary metal-oxide semiconductor (CMOS) compatible, silicon nanophotonic devices for monolithic on-chip integration of optical systems operating in telecom spectral regime where intrinsic bulk silicon has a negligible absorption. Such devices include for example low-loss nanoscale waveguides,[1−4] high-Q cavities,[5−7] high speed modulators,[8−11] and even light sources.[12,13] Yet, operating at the near-infrared transparency window limits the usefulness of silicon as an active absorbing material for photodetection. In order to develop all-silicon CMOS compatible photodetectors for on-chip optoelectronic integration, different approaches were proposed and demonstrated including two-photon absorption (TPA),[14,15] insertion of midbandgap defect states into silicon lattice,[16] using a polysilicon active layer,[17] cavity enhanced photocurrent generation,[15,17,18] and incorporation of germanium active layer with the silicon-based devices.[19−21] However, in the cases of germanium integration and introduction of midbandgap states into silicon lattice the main challenge remains to be the reduction of the dark current owing to the lattice mismatch and the presence of defects. On the other hand, using the nonlinear process (TPA) could potentially contribute to the low noise pure silicon photodetection, but this approach requires high optical power or realization of high quality factor optical cavity to achieve enhanced photon density.

An alternative way to detect infrared sub-bandgap optical radiation in silicon is to employ the internal photoemission (IPE) process using a Schottky barrier (SB) photodetector.[22−26] In its simplest form, such a detector consists of metal film on a lightly doped semiconductor (e.g., silicon) forming a Schottky contact at metal−semiconductor interface with potential barrier Φ_B and rectifying electrical characteristics. Typically, the obtained Schottky barrier (Φ_B) is lower than the energy bandgap of silicon,[23] thus allowing detection of long-wavelength (infrared) photons via the internal photoemission process. More specifically, when optical radiation below the bandgap is applied to the metal−silicon contact by top (through the metal) or back (through the semiconductor) illumination, the conduction electrons in the metal absorb infrared photons with the energy $h\nu$ exceeding the potential barrier at the interface Φ_B (see Figure 1). Gaining sufficient energy, these excited (hot) electrons are able to cross over the SB,[27] sweep out the depletion region of the semiconductor, and be collected as a photocurrent under reverse bias (photoconductive mode) operation.

The main advantages of SB photodetectors reside in their large bandwidth and simple fabrication process. However, since the volume in which the photons interact with electrons in the metal is very small, only a small fraction of the incident photons actually causes photoemission. To enhance the efficiency of the IPE process one would desire to directly guide light toward the active area of the detector and effectively confine the optical power at the boundary between the materials forming the Schottky contact, thereby increasing the interaction of light with the metal in the vicinity of the interface where the photoemission process

Received: January 17, 2011
Revised: May 6, 2011
Published: May 23, 2011

takes place. This light localization could significantly improve the detection capability of the system and potentially pave the way for device miniaturization and realization of on-chip photodetectors on the nanoscale. As early as in 1970s, the concept of using the high fields of the surface plasmon polaritons (SPP) on the metal−air interface for improving the efficiency of external photoemission in photocathodes has been explored,[28,29] and recently this concept had been successfully applied to the enhancement of internal photoemission for infrared photodetection in silicon-based plasmonic structures.[30−33] The SPP are optical surface waves propagating along the boundary between metal and dielectric where the electromagnetic fields decay evanescently in both media. While optical systems are basically diffraction limited, surface plasmons (SP) allow tight confinement of optical field to strongly subwavelength dimensions and provide guiding capabilities in nanoscale metallic structures.[34,35] Such properties are essential to achieve dense integration in the monolithic optoelectronic circuitry on-chip where a photodetector represents a basic building block of optical interconnect system.[36,37]

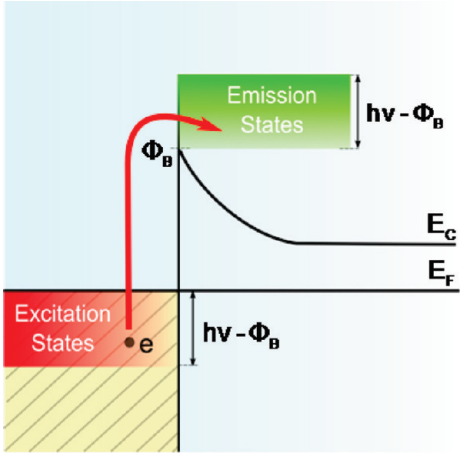

Figure 1. Energy band diagram of metal−semiconductor Schottky contact with the relevant states participating in the internal photoemission process. For simplicity, n-type contact is shown.

In this work, we present the on-chip nanoscale silicon surface-plasmon Schottky photodetector based on internal photoemission process and operating at telecom wavelengths. Our detector is fabricated using a self-aligned approach of local-oxidation of silicon (LOCOS) on silicon on insulator (SOI) substrate in which the nanoscale waveguide structure is defined by oxide spacers. Implementation of the LOCOS process provides compatibility with standard CMOS technology and permits a precise control over the shape and the dimensions of the waveguide.[4] Additionally, the LOCOS technique enables the fabrication of low-loss bus photonic waveguide (ca. 0.3 dB/cm) and the detector in the same process step, where the oxide spacers effectively define the area of metal−silicon interface and thus allow avoiding lateral misalignment between the silicon surface and the metal layer to form a Schottky contact.[38]

Figure 2 presents the fabrication process of on-chip optoelectronic link composed of photonic bus waveguide integrated with plasmonic Schottky detector. We used a 340 nm thick p-type silicon device layer ($\rho \sim 15\ \Omega \cdot$ cm) on top of a 2 μm thick buried oxide. First, a 100 nm of silicon nitride (SiN) was deposited by low-pressure chemical vapor deposition (LPCVD) at 800 °C to realize a protective layer for the LOCOS process. Next, the mask defining the optical and electrical structures including the photonic bus waveguide, the detection region, and the contacts area were patterned into the protective SiN layer using standard electron-beam lithography (EBL) followed by reactive ion etching (RIE) with a CHF_3/O_2 gas mixture. The defined pattern was next transferred to the silicon layer by wet oxidation process at 1000 °C where the nitride layer serves as a mask preventing the oxygen diffusion. After oxidation the nitride mask was removed by an additional RIE step. To make the Schottky plasmonic photodetector, we first realized an ohmic contact to the silicon layer by evaporating an aluminum pad and alloying the structure at 450 °C. Finally, a 50 nm thick Au layer was deposited onto the

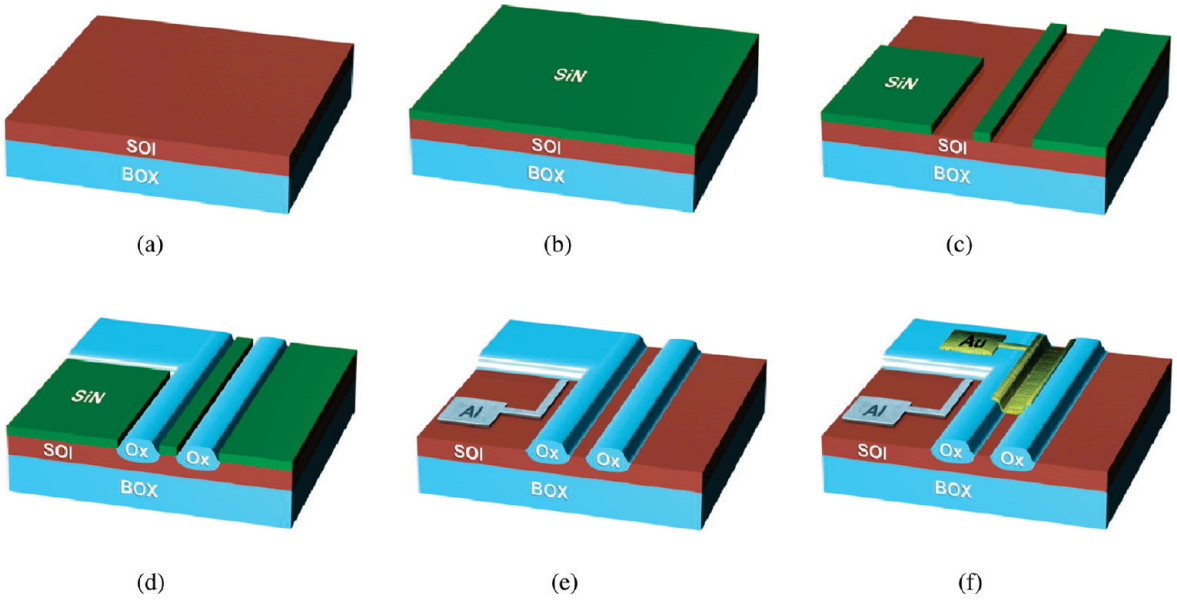

Figure 2. Fabrication process flow of the Schottky plasmonic photodetector integrated with photonic bus waveguide. (a) Planar SOI substrate; (b) nitride layer deposition; (c) nitride patterning; (d) local oxidation to define bus waveguide; (e) nitride strip and realization of ohmic contact to silicon; (f) formation of Schottky contact between silicon and Au layers.

dx.doi.org/10.1021/nl200187v |*Nano Lett.* 2011, 11, 2219–2224

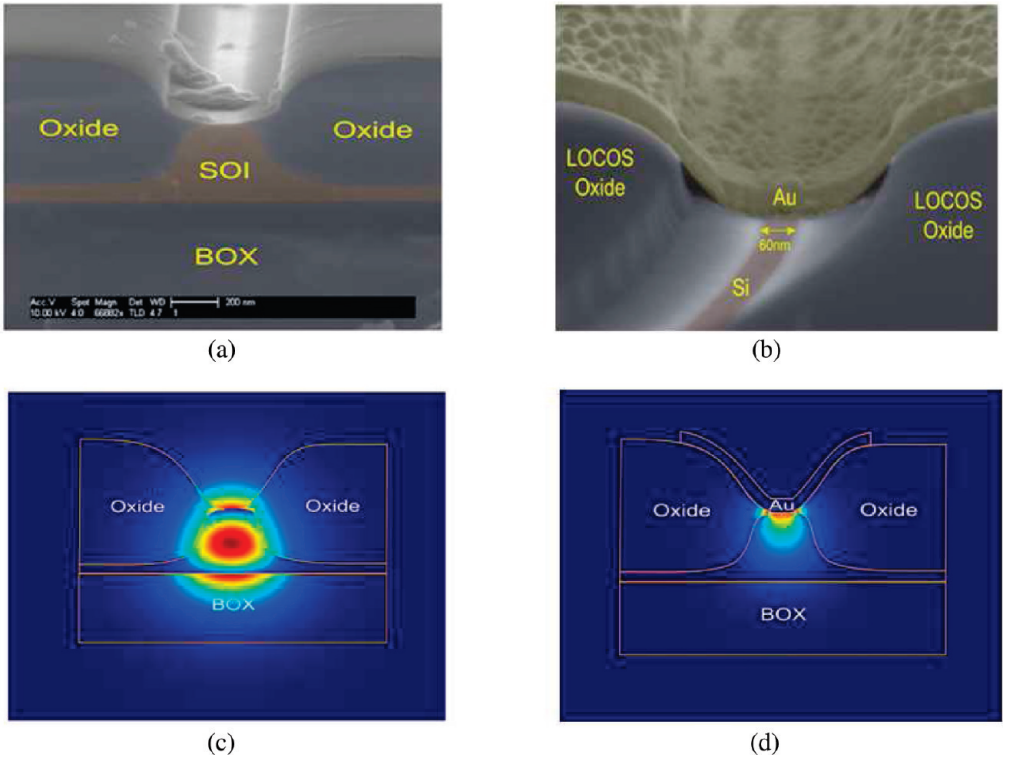

Figure 3. (a) SEM micrograph of the photonic bus waveguide after local-oxidation process before the metallization step; (b) SEM micrograph of the Schottky contact. (c) Intensity mode profile of the photonic bus waveguide. (d) Intensity mode profile of the plasmonic waveguide (Schottky contact).

chip (after short dip HF) followed by a lift-off process to lay down the metallic strip of the plasmonic structure to form a Schottky contact.

To find the profile of our structures following the LOCOS process, we captured scanning-electron microscope (SEM) micrographs of the photonic waveguide prior to metallization (Figure 3a) from which we obtained the dimensions of the bus waveguide to be 310 nm width and 340 nm height, supporting only a single transverse-magnetic (TM, out-of-plane) polarized optical mode. A thin rib (60 nm thickness) was kept to facilitate electrical contact to the silicon. According to Figure 3, the oxide spacers formed by the LOCOS process smooth the profile of the waveguide (Figure 3a) and provide an electrical isolation between the regions of high electric field generated at the sharp edges of metal and silicon (Figure 3b), thereby minimizing the leakage current of the device. On the basis of Figure 3b, we found the effective width of the detector to be 60 nm.

Next, using finite element mode solver (COMSOL) we calculated the optical mode profile of the silicon photonic bus waveguide and the plasmonic waveguide (e.g., Schottky contact) taking into account a subsequent deposition of 50 nm thick Au layer and the actual dimensions of the optical structure as taken from the SEM image (Figure 3c,d). According to the simulation results, the effective refractive index of the photonic and plasmonic nanowaveguides were found to be 2.29 and 3.25 + 0.02i, respectively.

Figure 4 shows the SEM image of the fabricated device. To ensure the inclusive absorption of the optical power in the detector, we used a 30 μm long SPP waveguide, much longer than the propagation length of SPP mode (~6 μm), which was calculated according to the 1/e intensity attenuation criterion and the simulation result of the complex refractive index. Additionally, we used a symmetric Y-splitter configuration to be able continuously monitor the optical signal in the detector by measuring the optical signal at the output facet of the chip.

To characterize the fabricated device, we first tested the electrical performance of the detector by measuring a current−voltage ($I-V$) characteristic of the Schottky contact. As demonstrated in Figure 5, the device shows the expected rectifying behavior with the forward bias region limited by the serial resistance of the contact and dark current in order of 13 nA for reverse bias of 0.1 V. To estimate the Schottky diode parameters, we measured the $I-V$ characteristics of the device for different temperatures and used the Arrhenius plot (I_0/T^2 vs $1/T$, where I_0 is the leakage current) for extracting the barrier height (Φ_B) and the effective Richardson constant (A^{**}). We found values of $\Phi_B = 0.315$ V and $A^{**} = 32 A/cm^2K^2$, very similar to the values presented in semiconductor textbooks[23] for (p-type)silicon−Au Schottky contact. We note that higher values of the barrier (as high as 0.7 eV)[39] were also reported for the same configuration. These differences may be the result of the high dependency on the fabrication process and specifically the surface treatment.

Next, we tested the detection capability of the device for different telecom wavelengths by measuring the $I-V$ characteristics of the Schottky diode at the presence of an optical signal. For this reason, a TM polarized light that originated from a diode laser was launched into the photonic bus waveguide using a polarization maintaining lensed fiber with a mode size of 2.5 μm. The light from the output facet of the waveguide was collected with a similar fiber and detected by power meter. By measuring the optical signal in the reference arm of the Y-splitter, we maximized the optical power in the Schottky detector by achieving a best alignment between the input/output tapered fibers and the bus waveguide.

dx.doi.org/10.1021/nl200187v |*Nano Lett.* 2011, 11, 2219–2224

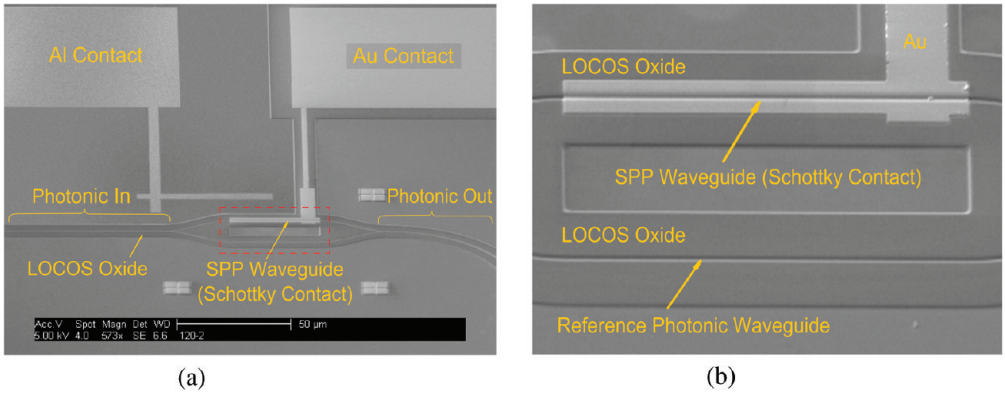

Figure 4. (a) SEM micrograph of the fabricated device; (b) zoom-in on the Schottky detector area, which is highlighted by the dashed red frame.

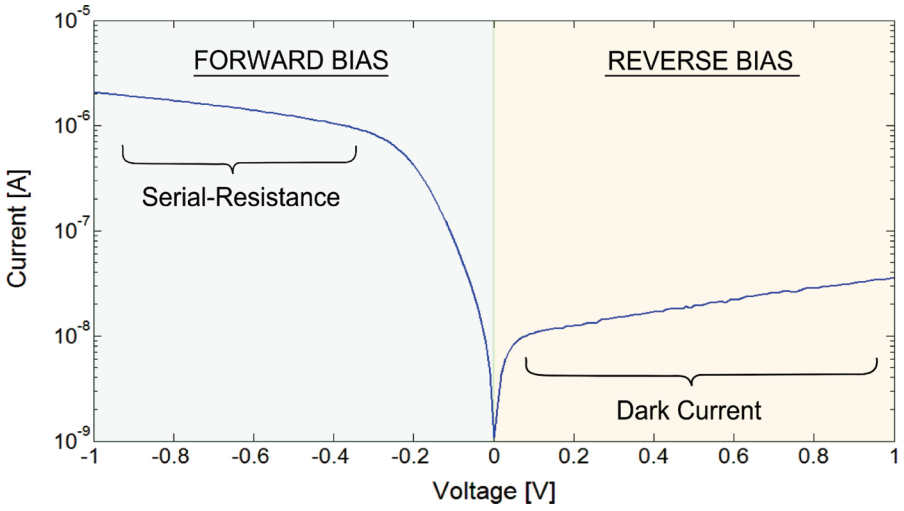

Figure 5. Current−voltage characteristic (semilogarithmic plot) of the fabricated Schottky photodetector. The dark current is 13 nA under reverse bias of 0.1 V.

Figure 6a represents the measurement results of the Schottky photodetector for optical signals at several wavelengths under constant incident optical power.

The observed spectral response reveals an increased responsivity for shorter wavelengths. This is expected due to the enhanced quantum efficiency of the internal photoemission process for energetic incident photons[27] according to the modified Fowler equation[27,40]

$$\eta = C\frac{(h\nu - \Phi_B)^2}{h\nu}$$

where η is the quantum efficiency of photoemission process (number of carriers that contribute to the photocurrent per incident photon) and C is the photoemission coefficient. The quadratic dependence essentially follows from the emission probability being proportional to both the density of metal electrons capable of surpassing the barrier and the density of empty states in the semiconductor accessible for these electrons (Figure 1). The obtained voltage dependence of the current in reverse bias can be related to the combined effect of SB lowering due to the image force and the space-charge-limited nature of the photocurrent.[23]

To determine the responsivity of the detector, we have measured the current across the Schottky contact under weak reverse bias of 0.1 V as a function of the incident optical power. A representative measurement result at the wavelength of 1.55 μm is shown in Figure 6b. As expected, the obtained photocurrent is increasing linearly with the increase in optical power, where the slope of the curve corresponds to detector responsivity according to $I = I_{dark} + RP_{in}$, where R is the detector responsivity and P_{in} is the incident optical power. To calculate the responsivity, we have first estimated the amount of optical power in SPP waveguide that contributes to the internal photoemission process. Taking into account the overall coupling loss of ~20 dB that is given by the coupling loss between tapered fiber and silicon waveguide (~10 dB) as well as the coupling loss from the bus silicon waveguide to the SPP waveguide (~10 dB), both calculated by mode (overlap integral) and impedance mismatch (Fresnel reflection), we estimated the maximal optical power within the Schottky detector to be in order of 15 μW for an incident laser power of 4 mW. Consequently, based on the measurement results presented in Figure 6a and P_{in} = 15 μW the responsivity of the device was found to be 0.25, 1.4, and 13.3 mA/W for optical wavelengths of 1.55, 1.47, and 1.31 μm, respectively. These responsivity values correspond to internal quantum efficiency of 2×10^{-4}, 1.2×10^{-3}, and 1.3×10^{-2}, respectively, which were calculated according to $\eta = (I_{ph}/q)/(P_{in}/h\nu)$, where I_{ph} is

dx.doi.org/10.1021/nl200187v |Nano Lett. 2011, 11, 2219–2224

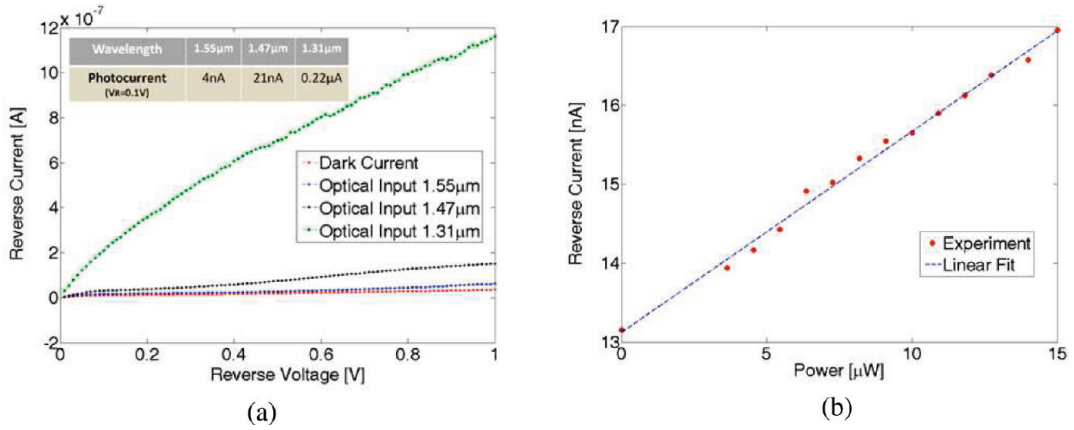

Figure 6. (a) $I-V$ curve in reverse bias for three different wavelengths in the near-infrared regime. (b) Representative result of responsivity measurement for wavelength of 1.55 μm. The current is measured under reverse bias of 0.1 V as a function of optical power in the Schottky detector.

the collected photocurrent, P_{in} is the optical power within the Schottky detector, q is a free electron charge and $h\nu$ is the energy of an incident photon. Because of low coupling efficiency between the lensed fiber and the Schottky detector (overall 20 dB loss) the external quantum efficiency is about 2 orders of magnitude lower than the internal one. The external quantum efficiency could be enhanced by improving the coupling condition from the external fiber to the photonic bus waveguide (e.g., by the use of the inverse taper approach) and by allowing an adiabatic transition from the photonic to the plasmonic structure. Finally, using the responsivity values for different wavelengths with corresponding photon energies we have used the Fowler plot[27,40] and verified that the measurement results do follow the linear dependence of $R^{1/2} h\nu \propto (h\nu - \Phi_B)$.

In summary, we experimentally demonstrated an on-chip configuration of optoelectronic link composed of photonic bus waveguide integrated with locally oxidized nanoscale silicon surface-plasmon Schottky detector for the telecom spectral regime. Implementation of the LOCOS process allows a precise control over the shape and the dimensions of the photonic structure and enables the fabrication of low-loss bus waveguide and the detector in the same process step. The fabricated device showed enhanced detection capability for shorter wavelengths that is attributed to the increased probability of the internal photoemission process. We found the responsivity of the detector to be 0.25, 1.4, and 13.3 mA/W for incident optical wavelengths of 1.55, 1.47, and 1.31 μm, respectively. On the basis of $I-V$ characteristics, we found the barrier height at metal/silicon interface to be 0.315 eV. We believe that demonstrated device is a step forward in merging silicon nanophotonic and silicon plasmonic platforms with the major advantage of using silicon nanostructures for the detection of optical signals in the telecom regime.

AUTHOR INFORMATION

Corresponding Author
*E-mail: ulevy@cc.huji.ac.il.

Author Contributions
§These authors contributed equally to the work.

ACKNOWLEDGMENT

We acknowledge a technical support of David Shlosberg and Noa Mazursky. The research was supported U.S.—Israel Binational science foundation. I.G. acknowledges financial support from the Eshkol Fellowship and the Lillian and Bryant Shiller Ph. D Fellowship in Applied Physics. The devices were fabricated at the Center for Nanoscience and Nanotechnology, The Hebrew University of Jerusalem.

REFERENCES

(1) Cardenas, J.; Poitras, C. B.; Robinson, J. T.; Preston, K.; Chen, L.; Lipson, M. Low loss etchless silicon photonic waveguides. *Opt. Express* **2009**, *17*, 4752–4757.

(2) Sherwood-Droz, N.; Gondarenko, A.; Lipson, M. Oxidized Silicon-On-Insulator (OxSOI) from bulk silicon: a new photonic platform. *Opt. Express* **2010**, *18*, 5785–5790.

(3) Milošević, M. M.; Mashanovich, G. Z.; Gardes, F. Y.; Hu, Y.; Knights, A. P.; Tarr, N. G.; Reed, G. T. Athermal and low loss ridge silicon waveguides. *Proc. SPIE* **2010**, *76*, 061A.

(4) Desiatov, B.; Goykhman, I.; Levy, U. Demonstration of submicron square-like silicon waveguide using optimized LOCOS process. *Opt. Express* **2010**, *18*, 18 592–18 597.

(5) Velha, P.; Picard, E.; Charvolin, T.; Hadji, E.; Rodier, J. C.; Lalanne, P.; Peyrade, D. Ultra-High Q/V FabryPerot microcavity on SOI substrate. *Opt. Express* **2007**, *15* (24), 16090–16096.

(6) Kuramochi, E.; Taniyama, H.; Tanabe, T.; Kawasaki, K.; Roh, Y.-G.; Notomi, M. Ultrahigh-Q one-dimensional photonic crystal nanocavities with modulated mode-gap barriers on SiO_2 claddings and on air claddings. *Opt. Express* **2010**, *18* (15), 15 859–15 869.

(7) Gondarenko, A.; Levy, J. S.; Lipson, M. High confinement micron-scale silicon nitride high Q ring resonator. *Opt. Express* **2009**, *17*, 11366–11370.

(8) Xu, Q.; Manipatruni, S.; Schmidt, B.; Shakya, J.; Lipson, M. 12.5 Gbit/s carrier-injection-based silicon micro-ring silicon modulators. *Opt. Express* **2007**, *15*, 430–436.

(9) Liu, A.; Liao, L.; Rubin, D.; Nguyen, H.; Ciftcioglu, B.; Chetrit, Y.; Izhaky, N.; Paniccia, M. High-speed optical modulation based on carrier depletion in a silicon waveguide. *Opt. Express* **2007**, *15*, 660–668.

(10) Reed, G. T.; Mashanovich, G.; Gardes, F. Y.; Thomson, D. J. Silicon optical modulators. *Nat. Photonics* **2010**, *4* (8), 518–526.

(11) Green, W. M.; Rooks, M. J.; Sekaric, L.; Vlasov, Y. A. Ultra-compact, low RF power, 10 Gb/s siliconMach-Zehnder modulator. *Opt. Expres* **2007**, *15* (25), 17 106–17 113.

(12) Rong, H.; Liu, A.; Jones, R.; Cohen, O.; Hak, D.; Nicolaescu, R.; Fang, A.; Paniccia, M. An all-silicon Raman laser. *Nature* **2005**, *433* (7023), 292–294.
(13) Liang, D.; Bowers, J. E. Recent progress in lasers on silicon. *Nat. Photonics* **2010**, *4* (8), 511–517.
(14) Liang, T. K.; Tsang, H. K.; Day, I. E.; Drake, J.; Knights, A. P.; Asghari, M. Silicon waveguide two-photon absorption detector at 1.5μm wavelength for autocorrelation measurements. *Appl. Phys. Lett.* **2002**, *81* (7), 1323–1325.
(15) Tanabe, T.; Sumikura, H.; Taniyama, H.; Shinya, A.; Notomi, M. All-silicon sub-Gb/s telecom detector with low dark current and high quantum efficiency on chip; http://arxiv.org/abs/1002.3207.
(16) Bradley, J. D. B.; Jessop, P. E.; Knights, A. P. Silicon waveguide-integrated optical power monitor with enhanced sensitivity at 1550 nm. *Appl. Phys. Lett.* **2005**, *86* (24), 241 103.
(17) Preston, K.; Lee, Y. H.; Zhang, M.; Lipson, M. Waveguide-integrated telecom-wavelength photodiode in deposited silicon. *Opt. Lett.* **2011**, *36* (1), 52–54.
(18) Chen, H.; Luo, X.; Poon, A. W. Cavity-enhanced photocurrent generation by 1.55 μm wavelengths linear absorption in a p-i-n diode embedded silicon microring resonator. *Appl. Phys. Lett.* **2009**, *95* (17), 171 111.
(19) Kang, Y.; Liu, H.-D.; Morse, M.; Paniccia, M. J.; Zadka, M.; Litski, S.; Sarid, G.; Pauchard, A.; Kuo, Y.-H.; Chen, H.-W.; Zaoui, W. S.; Bowers, J. E.; Beling, A.; McIntosh, D. C.; Zheng, X.; Campbell, J. C. Monolithic germanium/silicon avalanche photodiodes with 340 GHz gain−bandwidth product. *Nat. Photonics* **2008**, *3* (1), 59–63.
(20) Assefa, S.; Xia, F.; Vlasov, Y. A. Reinventing germanium avalanche photodetector for nanophotonic on-chip optical interconnects. *Nature* **2010**, *464* (7285), 80–84.
(21) Michel, J.; Liu, J.; Kimerling, L. C. High-performance Ge-on-Si photodetectors. *Nat. Photonics* **2010**, *4* (8), 527–534.
(22) Peters, D. W. An infrared detector utilizing internal photoemission. *Proc. IEEE* **1967**, *55* (5), 704–705.
(23) Sze, S. M.; Ng, K. K. *Physics of Semiconductor Devices*; Wiley: New York, 2006.
(24) Zhu, S.; Yu, M. B.; Lo, G. Q.; Kwong, D. L. Near-infrared waveguide-based nickel silicide Schottky-barrier photodetector for optical communications. *Appl. Phys. Lett.* **2008**, *92* (8), 081 103.
(25) Casalino, M.; Sirleto, L.; Iodice, M.; Saffioti, N.; Gioffrè, M.; Rendina, I.; Coppola, G. Cu/p-Si Schottky barrier-based near infrared photodetector integrated with a silicon-on-insulator waveguide. *Appl. Phys. Lett.* **2010**, *96* (24), 241 112.
(26) Li, S.; Tarr, N. G.; Berini, P. Schottky photodetector integration on LOCOS-defined SOI waveguides. *Proc. SPIE* **2010**, *7750*, 77501M–77501M-9.
(27) Scales, C.; Berini, P. Thin-Film Schottky Barrier Photodetector Models. *IEEE J. Quantum Elect.* **2010**, *46* (5), 633–643.
(28) Endriz, J. G. Surface waves and grating-tuned photocathodes. *Appl. Phys. Lett.* **1974**, *25*, 261–262.
(29) Sipe, J. E.; Becher, J. Surface-plasmon-assisted photoemission. *J. Opt. Soc. Am.* **1981**, *71* (10), 1286–1288.
(30) Akbari, A.; Berini, P. Schottky contact surface-plasmon detector integrated with an asymmetric metal stripe waveguide. *Appl. Phys. Lett.* **2009**, *95* (2), 021 104.
(31) Wang, Y.; Su, X.; Zhu, Y.; Wang, Q.; Zhu, D.; Zhao, J.; Chen, S.; Huang, W.; Wu, S. Photocurrent in Ag-Si photodiodes modulated by plasmonic nanopatterns. *Appl. Phys. Lett.* **2009**, *95* (24), 241 106.
(32) Akbari, A.; Tait, R. N.; Berini, P. Surface plasmon waveguide Schottky detector. *Opt. Express* **2010**, *18* (8), 8505–8514.
(33) Dufaux, T.; Dorfmüller, J.; Vogelgesang, R.; Burghard, M.; Kern, K. Surface plasmon coupling to nanoscale Schottky-type electrical detectors. *Appl. Phys. Lett.* **2010**, *97* (16), 161 110.
(34) Gramotnev, D. K.; Bozhevolnyi, S. I. Plasmonics beyond the diffraction limit. *Nat. Photonics* **2010**, *4* (2), 83–91.
(35) Schuller, J. A.; Barnard, E. S.; Cai, W.; Jun, Y. C.; White, J. S.; Brongersma, M. L. Plasmonics for extreme light concentration and manipulation. *Nat. Mater.* **2010**, *9* (3), 193–204.
(36) Ozbay, E. Plasmonics: Merging Photonics and Electronics at Nanoscale Dimensions. *Science* **2006**, *311* (5758), 189–193.
(37) Miller, D. A. B. Device Requirements for Optical Interconnects to Silicon Chips. *Proc. IEEE* **2009**, *97* (7), 1166–1185.
(38) Goykhman, I.; Desiatov, B.; Levy, U. Experimental demonstration of locally oxidized hybrid silicon-plasmonic waveguide. *Appl. Phys. Lett.* **2010**, *97* (14), 141106.
(39) Yeganeh, M. A.; Rahmatollahpur, S. H. Barrier height and ideality factor dependency on identically produced small Au/p-Si schottky barrier diodes. *J. Semicond.* **2010**, *31* (7), 07400.
(40) Fowler, R. H. The analysis of photoelectric sensitivity curves for clean metals at various temperatures. *Phys. Rev.* **1931**, *38* (1), 45–56.